# ULTRA HIGH RESOLUTION ION BEAM PROCESSES

R.L. Seliger, J.W. Ward, and D. Hunken

Hughes Research Laboratories
3011 Malibu Canyon Road
Malibu, CA 90265

December 1976

Semiannual Progress Report 1
1 May 1976 – 31 October 1976

Prepared For
NAVAL ELECTRONICS LABORATORY CENTER
271 Catalina Boulevard
San Diego, CA 92152

UNCLASSIFIED

SECURITY CLASSIFICATION OF THIS PAGE (When Data Entered)

| REPORT DOCUMENTATION PAGE | | READ INSTRUCTIONS BEFORE COMPLETING FORM |
|---|---|---|
| 1. REPORT NUMBER | 2. GOVT ACCESSION NO. AD-A155 | 3. RECIPIENT'S CATALOG NUMBER 749 |
| 4. TITLE (and Subtitle) ULTRAHIGH RESOLUTION ION BEAM PROCESSES | | 5. TYPE OF REPORT & PERIOD COVERED Semiannual Prog. Rpt. 1 1 May 1976-31 Oct. 1976 |
| | | 6. PERFORMING ORG. REPORT NUMBER |
| 7. AUTHOR(s) R.L. Seliger, J.W. Ward, and D. Hunken | | 8. CONTRACT OR GRANT NUMBER(s) N00123-76-C-1199 |
| 9. PERFORMING ORGANIZATION NAME AND ADDRESS Hughes Research Laboratories 3011 Malibu Canyon Road Malibu, CA 90265 | | 10. PROGRAM ELEMENT, PROJECT, TASK AREA & WORK UNIT NUMBERS ARPA Order No. 3254 |
| 11. CONTROLLING OFFICE NAME AND ADDRESS Naval Electronics Laboratory Center 271 Catalina Boulevard San Diego, CA 92152 | | 12. REPORT DATE December 1976 |
| | | 13. NUMBER OF PAGES |
| 14. MONITORING AGENCY NAME & ADDRESS(if different from Controlling Office) | | 15. SECURITY CLASS. (of this report) UNCLASSIFIED |
| | | 15a. DECLASSIFICATION DOWNGRADING SCHEDULE |

16. DISTRIBUTION STATEMENT (of this Report)

17. DISTRIBUTION STATEMENT (of the abstract entered in Block 20, if different from Report)

18. SUPPLEMENTARY NOTES

20

19. KEY WORDS (Continue on reverse side if necessary and identify by block number)

Ion Beam,
Sputtering,
Focusing Column,
Einzel Lens

| Accession For | |
|---|---|
| NTIS GRA&I | ☒ |
| DTIC TAB | ☐ |
| Unannounced | ☐ |
| Justification | |
| By | |
| Distribution/ | |
| Availability Codes | |
| Dist | Avail and/or Special |
| A/1 | |

DTIC COPY INSPECTED

20. ABSTRACT (Continue on reverse side if necessary and identify by block number)

This is the first semiannual progress report on the program "Ultra-high Resolution Ion Beam Processes." The overall goal of the program is to establish the technical and economic feasibility of applying submicrometer diameter focused ion beams to microcircuit fabrication without the use of masks. The progress for this reporting period consists of obtaining and operating two high brightness ion

DD FORM 1 JAN 73 1473 EDITION OF 1 NOV 65 IS OBSOLETE

UNCLASSIFIED

SECURITY CLASSIFICATION OF THIS PAGE (When Data Entered)

sources, analyzing focusing lenses and columns, and designing and fabricating a focusing column for each ion source. These columns are now about 80% complete and it is expected that one will be put into operation during the next quarter.

## TABLE OF CONTENTS

## LIST OF ILLUSTRATIONS

# I. INTRODUCTION AND SUMMARY

This is the first semiannual report on the program "Ultrahigh Resolution Ion Beam Processes – Phase I." The overall goal of the program is to establish the technical and economic feasibility of applying submicrometer diameter focused ion beams to microcircuit fabrication without the use of masks. Fabrication processes being considered are ion machining, resist exposure, and implantation doping. The program is comprised of two main parts, one experimental, the other analytical. The experimental investigation is directed at evaluating two high brightness ion sources – a gas field ionization (GFI) source and a liquid metal plasma (LMP) source. Both sources will be set up in simple focusing columns with the goal of demonstrating submicrometer focused spots. The ion source investigation will evaluate the economic feasibility of using focused ion beams. The analytical investigation is aimed at designing optimized focusing columns for each ion source. The analysis will determine the expected performance of these optimized columns (e.g., *spot current versus spot size*) for the various microfabrication processes: ultrahigh resolution machining, resist exposure, and doping. The program will conclude with the conceptual design of a focusing system together with its predicted performance (optimized for a specific application). The decision to begin Phase II, the building of a laboratory prototype, will be based on the predicted performance.

Significant progress was made in the experimental and analytical investigations. Both the LMP and GFI ion sources were set up and operated. A process for fabricating tungsten needles for the LMP source was developed. The total current measured from one of these needles was typically 40 μA at 6 kV. When apertured to an angle of 10 mrad, a current of 5 nA was collected. With a virtual source size of 500 A diameter, as was reported by Krohn at the Argonne National Laboratory, the source brightness is $10^6$ A/cm$^2$-sr, a value comparable to a high brightness $LaB_6$ electron emitter. The GFI source has been operated only briefly thus far, but preliminary data agreed with that obtained by Orloff at the Oregon Graduate Center. Under the analytical part of the program, an electrostatic lens computer program was

obtained and used to evaluate various lens designs. Two focusing column configurations, for which the computer analysis predicts sub-micrometer diameter focused spots, were chosen for experimental testing: a double enzel lens column for the GFI source and a single accelerating lens column for the LMP source. The mechanical design and construction of these focusing columns is about 80% complete. It is expected that the GFI column will be put into full operation during the next quarter. Thus far, no technical problems have been uncovered that would impair meeting the original program schedule or goals.

## II. EXPERIMENTAL INVESTIGATION

During the first six months, a major effort was made to launch the experimental portion of the program. The activities pursued included (1) procurement, setup, and operation of two high brightness ion sources – a liquid metal plasma (LMP) and a gas field ionization (GFI) source; (2) design and fabrication of two focusing columns; and (3) re-design and fabrication of a liquid metal plasma ion source. The fabrication and assembly of the focusing columns and new LMP source are now approximately 80% complete. The first focusing experiments are expected to take place during the next quarter.

### A. Ion Source Evaluation

The first phase of our evaluation of the LMP and GFI sources was to test them at the reported operating points and evaluate their suitability for integrating with focusing columns. Since the GFI source is well known and is now being operated in a focusing column (by Jon Orloff), our initial evaluation was brief. We simply reproduced the expected current versus voltage characteristics. With the LMP source, however, there are many unanswered questions concerning its suitability for focusing, and consequently our initial evaluation was more extensive.

#### 1. Initial Operation of the GFI Source

Photographs of the GFI source are shown in Figure II-1. Gas to be ionized enters the feed tube and fills the cylindrical volume enclosed by the extraction cup and lower glass chamber to a pressure of about $10^{-2}$ Torr. A very sharp needle (radius 1000 to 2000 Å) is oriented on the axis of the pressurized volume with its tip 1 mm from the end of the extraction cup. A 0.5 mm diameter aperture located on axis in the end of the cup allows the field ionization current that originates at the tip to enter the main vacuum envelope, where the pressure is much reduced (e.g., $10^{-6}$ Torr). Thus, the extraction

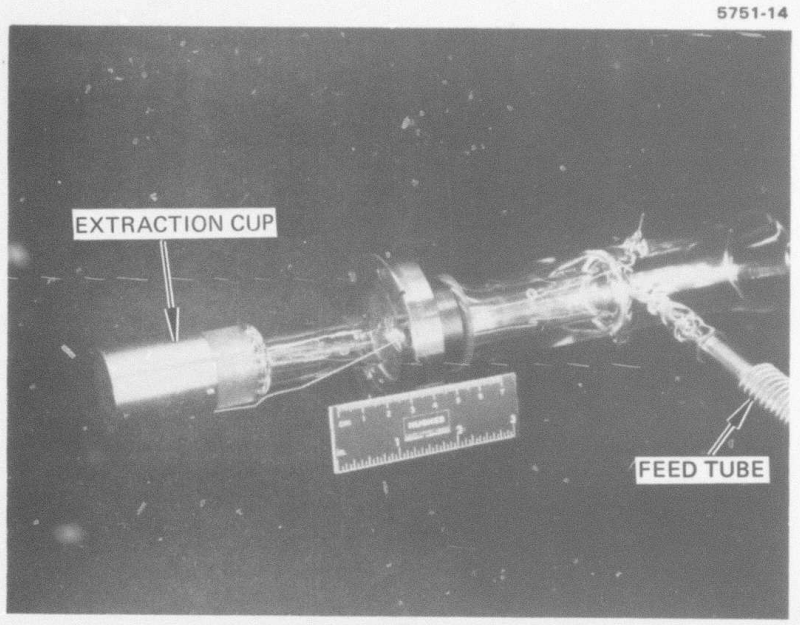


(a)

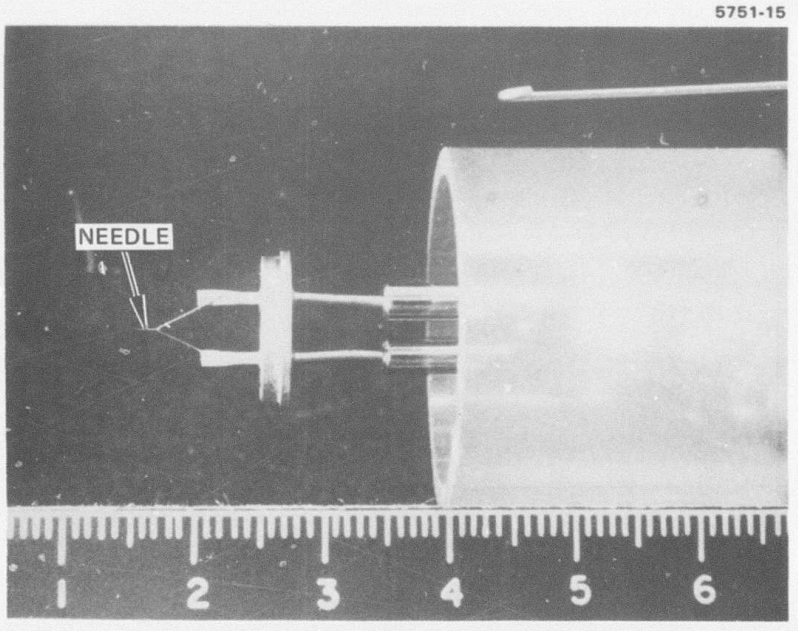


(b)

Figure II-1. Gas field ionization source.
(a) Complete assembly
(b) Tip region

aperture serves as a differential pumping port, which causes a high tip current (proportional to pressure) and a hard vacuum downstream. These, in turn, enable ion beam transport through focusing lenses, deflectors, etc. without scattering. The field ionization process has been described in great detail[1] and will not be repeated here. It is sufficient just to mention that applying a positive voltage of 10 to 15 kV to the tip with the extraction-cup grounded produces an ion current on the order of $10^{-7}$ A. The ion trajectories nominally fill a cone of about $40^{o}$ included angle and appear to all emanate from a very small area. This effective emission area is known as the "virtual source". The diameter of the virtual source for a field ionization source is very small (<100Å) and its contribution to the diameter of a focused spot will be negligible compared with the effects of lens aberrations.

The GFI source was set up in a glass cross on a diffusion pump vacuum station. The major part of setup time was spent in building the gas feed system. A schematic of the feed system is shown in Figure II-2. Data from its initial operation, presented in Figure II-3, is in good agreement with that reported for field ionization sources. That is, a two-slope I versus V characteristic was measured which corresponds first to increasing ionization probability with voltage (steep slope) and then to increasing dipole attraction of the gas with increased tip voltage. No attempt to maximize the source current was made, since such efforts would not really be significant until the source is tested in the focusing column.

### 2. Initial Operation of the LMP Source

A gallium LMP source was purchased from Culham Laboratory and was set up in a glass cross on an oil diffusion pump vacuum station for initial testing. The LMP source is shown schematically in Figure II-4(a), and a photograph is shown in Figure II-4(b). The source employed a 0.25 x 50 mm tungsten wire needle that is sharpened at one end to a 1 to 5 μm radius point. This needle was almost completely inserted into a 6 mm diameter cylindrical reservoir filled with gallium. An extraction electrode with a 3 mm diameter

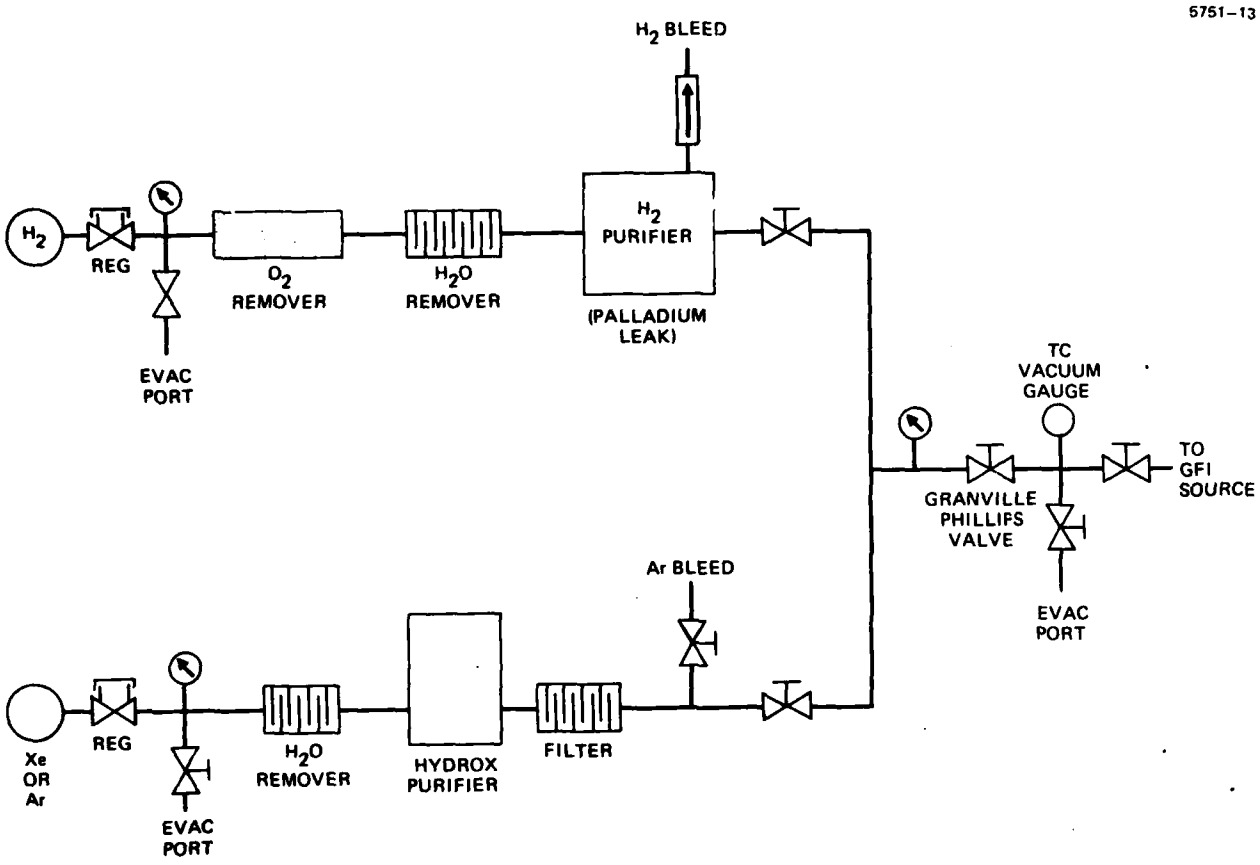


Figure II-2. Gas feed system for the GFI source.

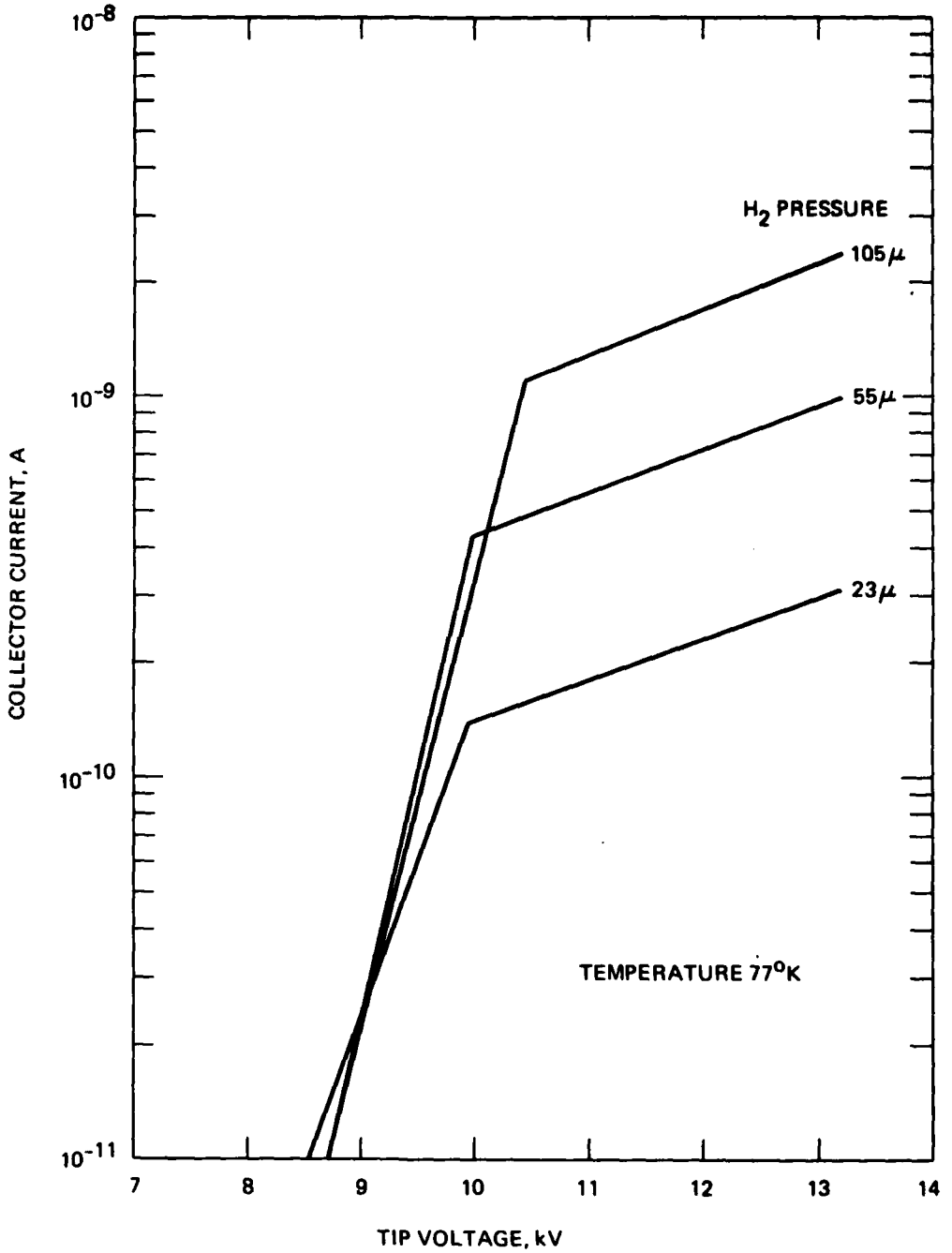


Figure II-3. GFI source I versus V characteristics.

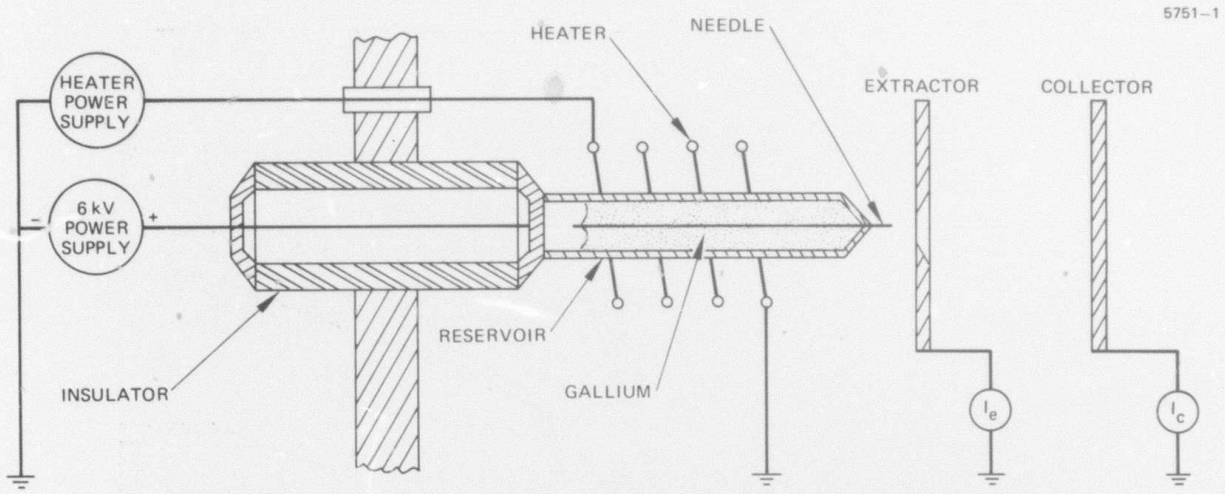


(a) Schematic of the LMP source.

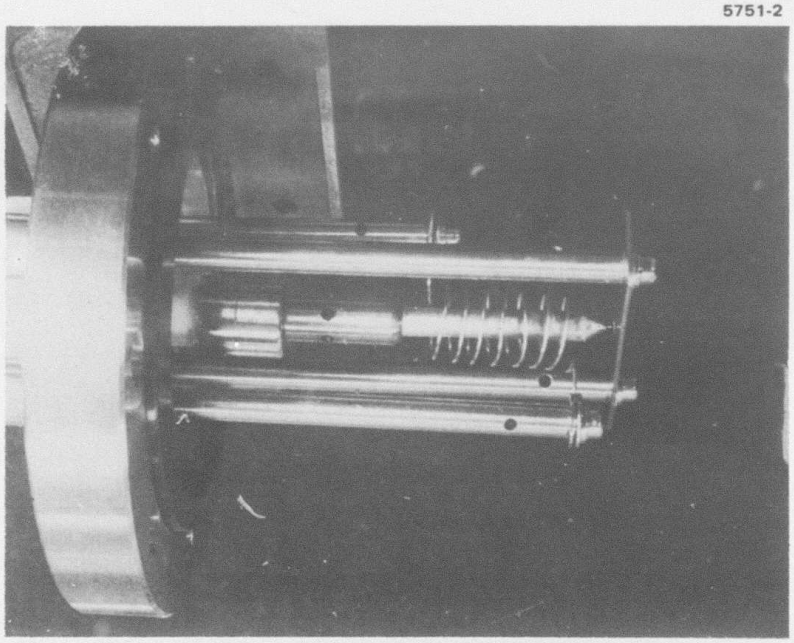


(b) Photograph of LMP source.

Figure II-4. LMP source.

aperture was mounted just downstream of the needle. A wire coil of ~15 mm overall diameter was mounted coaxially with the reservoir for radiant heating. Source startup typically consisted of heating the reservoir for 15 min and then applying a positive voltage to the needle-reservoir assembly.

The LMP source operated erratically with the original needle supplied, so we developed a procedure for fabricating new needles. (It was later determined that the tip of the original needle was damaged.) The needle fabrication procedure is described in Appendix A.

The best source performance was obtained with needles of ~5 μm radius. The ionization mechanism in this source is not well understood. It appears that under proper operation the electric field creates a cusp of liquid Ga at the end of the needle and that a continuous flow of liquid Ga along the tungsten wire is set up to maintain this cusp. With very sharp needles (e.g., 0.25 μm radius), the flow was unstable and the current drifted. However, with 5 μm radius needles, the source emitted currents of 40 μA at 6 kV for many hours (e.g., three 8-hour days).

### 3. Mass Analysis of the Ga Beam

The Ga beam was mass analyzed, primarily to determine if the beam contained charged droplets (ion clusters) or just $Ga^+$ ions. An existing ExB mass analyzer was used; Figure II-5 shows the mass spectrum obtained. The large peak corresponds to $Ga^+$, and no evidence of ion clusters was found.

### 4. Intensity of the Ga Beam

The final measurement made on the LMP source was of the current that would enter a focusing column. A 0.5 mm diameter aperture was located 25 mm from the needle to simulate a 10 mrad column acceptance angle. The current transmitted through the aperture varied between 5 and 9 nA as total current varied between 15 and 40 μA. Although this is a substantial current, spot size will depend on the diameter of the active source area from which the current originates.

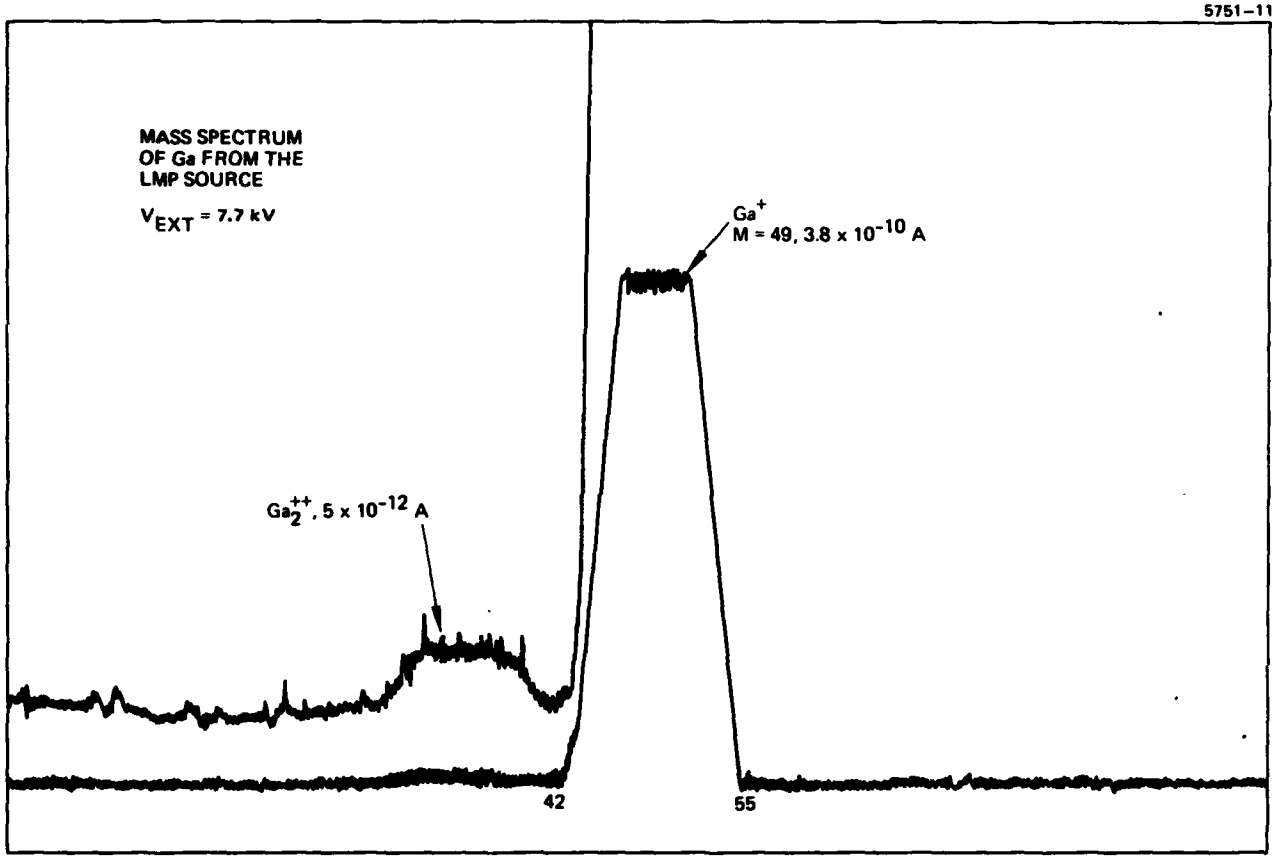


Figure II-5. Mass spectrum from the Ga-LMP source..

For our focusing applications it is important that the effective source size be less than or equal to $d_s/M$, where $d_s$ is the focused spot size and M is the magnification. Thus, if M = 1 and we want $d_s$ = 0.25 μm, the effective source size should be <0.25 μm.

A preliminary but important conclusion from the initial operation of the LMP source is that it is sufficiently stable and reproducible to permit a critical evaluation in a focusing column. The remaining efforts in ion source evaluation will be made after the focusing columns are completed and operating.

## B. Focusing Column Design and Fabrication

The major criteria used to choose a focusing column for fabrication were that the

- Lenses be high quality (i.e., have low aberrations)
- Lenses had been evaluated previously
- Column be as simple as possible (e.g., contain the fewest lenses) but be capable of producing sub-micrometer spots
- Column enable a comprehensive evaluation of the suitability of the high brightness ion source to fine focusing and microfabrication.

### 1. Choice of Focusing Column for Fabrication

After studying information gained during the literature survey, it appeared quite likely that two focusing columns could meet the above criteria: a two-einzel lens column and a single-accelerating lens column. Both these columns have been used successfully for focusing the electron beam from field emission electron sources. In particular, Wall, Welter, and Crew[2] employed a single accelerating lens column in their early work (1968). The same approach was later used by Coats and Welter[3] in commercially produced field-emission gun scanning electron microscopes. On the other hand, Wolf[4] produced excellent results using a two-lens column to image a thermal-field

emitter electron source for a micro-recording system application. Thus, from our analysis and the electron beam results, both columns are highly credible candidates for imaging our high-field ion sources.

Therefore, we decided that it would be profitable to fabricate two separate focusing columns (one of each type) so that their relative merits for ion beam focusing could be compared. With two focusing columns being fabricated, we had to decide which ion source should be integrated with which column or whether the columns should be engineered to accept both sources.

### 2. Matching Ion Sources and Focusing Columns

There is no fundamental reason why both focusing columns could not be designed to accept both the LMP and GFI ion sources. However, to reduce engineering costs, we decided to fit one ion source to each column.

The matching of individual ion sources and focusing columns was then based on several considerations, including engineering simplification and cost reduction. Table II-1 presents the reasons for the final choice, which was to integrate the GFI source with the double-einzel lens column and the LMP source with the single accelerating lens column. Thus, the goal of this program – to evaluate each high brightness ion source by imaging it into a submicron spot – will be achieved using two experimental setups in which engineering complexity is minimized.

### 3. Design of the GFI Focusing Column

Since the two-einzel lens focusing column will henceforth be associated with the GFI source, we will call the combination the GFI column. A large fraction of the program effort during the

Table II-1. Matching Ion Sources and Focusing Columns

| |
|---|
| GFI Source – 2 Einzel Lens Column (Focused beam energy determined by extraction voltage) |
| • GFI extraction voltage (~12kV to 30kV) sufficently high for $H^+$ lithography and $Ar^+$ sputtering |
| • Gas feed system and $LN_2$ reservoir for GFI source preferably at laboratory ground potential |
| LMP Source – Single Accelerating Lens Column (Focused beam energy determined by 10x the source extraction voltage) |
| • LMP extraction voltage (6 – 10 kV) is half that for the GFI source. Thus, the 10x acceleration results in only modestly high overall system voltages (60-100kV) |
| • Very simple source requirements, e.g., only one Ga heater that must be operated at high voltage. |
| • Increased $Ga^+$ voltage desirable for demonstrating ion implantation of heavy ions with some depth of penetration (i.e., range). |

second quarter was devoted to designing and fabricating the GFI column. Some of the main design objectives were to

- Employ precision-made einzel lenses
- Implement a method of mounting the lenses coaxially (thereby defining a column axis)
- Provide a mounting flange for the ion source that could be moved with the column in operation for transverse alignment of the source with the column axis.

Figure II-6 is a schematic of the GFI column. The GFI source (described previously) was mounted on a flange supported by the ion source alignment bearing. Four actuators were used to position and lock the source on to the column axis. The bellows vacuum seal between

the mounting flange and the remaining column allows performing this alignment with the column in full operation. The two einzel lenses (one denoted the objective and other the projector lens in Figure II-6) are of the same design and are machined to concentricity tolerances of less than 0.0001 in. The lenses were purchased from Electros Inc., where the design had been developed for a transmission electron microscope. The performance data for these lenses, given in Figure III-4, was also furnished. The lenses were oriented in the column such that the source (virtual object) was at the focal distance of the objective lens and the target is at the focal distance of the projector lens. The ion beam trajectories are parallel between the lenses; the lens separation is not critical.

An alignment "V-block" was used to mount the two einzel lenses coaxially. The V-block was formed by fastening two flat rectangular bars at a $90^{o}$ angle. Precision is determined by the flatness of the inside faces of the bars. We had these faces ground and lapped flat to a 0.0001 in. tolerance. The intersection of the planes of the faces forms a straight line parallel to the column axis. The einzel lens elements are contained in concentric cylindrical holders; these holders have a very accurately machined outside diameter. Thus, when the lenses are set in the V-block their axes should lie on the same line. The length of the V-block (~15 in.) was chosen to allow accurate coaxial mounting of other ion optical elements such as apertures, steering plates, a deflection system, and a stigmator.

The target region makes up the remainder of the GFI column. A gate valve was incorporated between the target chamber and the upper column so that target changes could be made without venting the ion source. This approach is particularly beneficial for the GFI source cooled by $LN_2$. The target stage has two mechanisms for XY positioning. Coarse X, Y, and Z positioning is accomplished by lead screw slide drives with actuator shafts coupled through the vacuum wall. A second electromechanical (piezoelectric) XY target scanner will be programmed to scan the target beneath the stationary ion beam. This target scanning

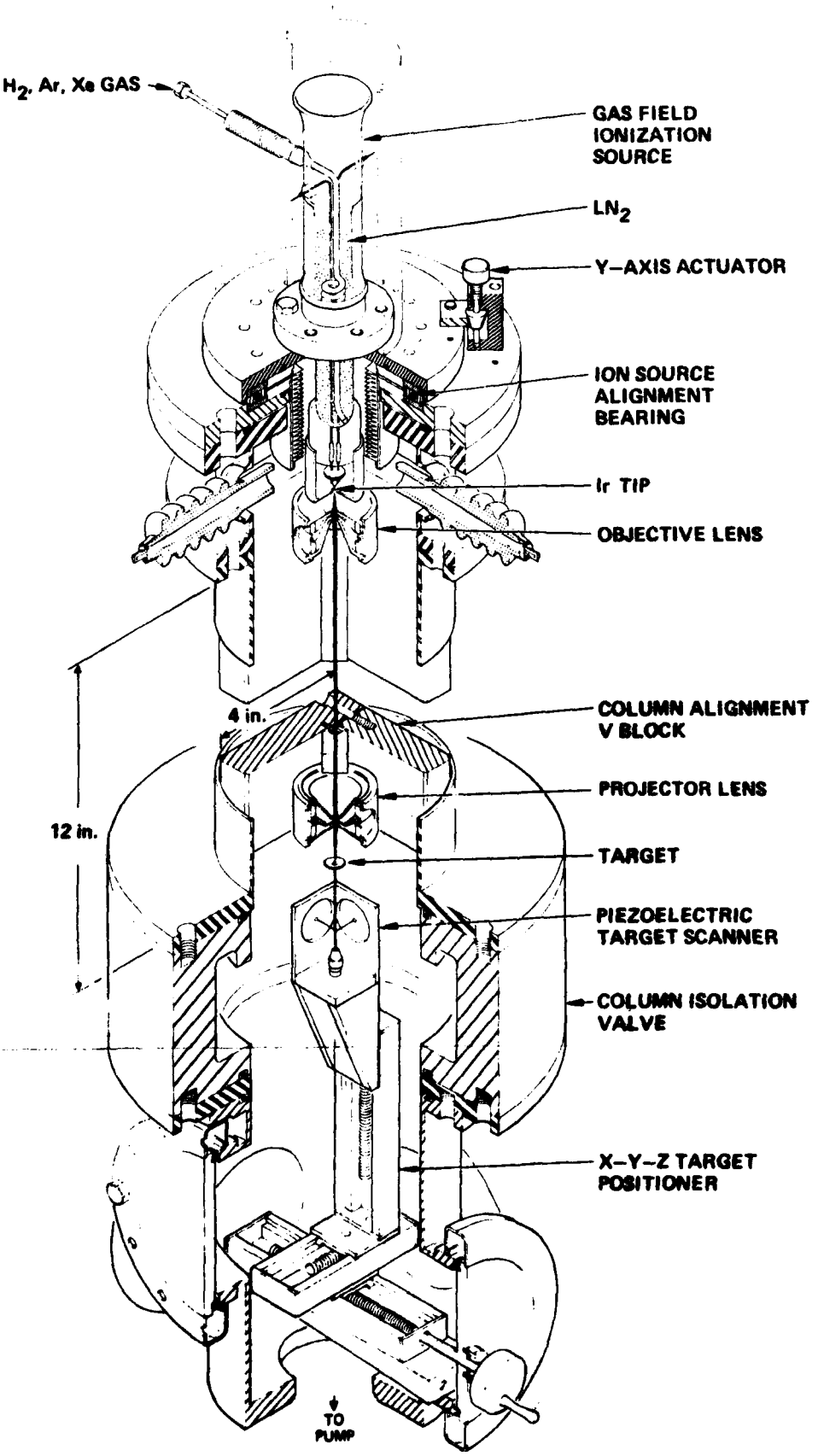


Figure II-6. CFI focusing column.

method will be only a temporary substitute for electrostatic beam scanning, a method which is far more complex but is necessary for microfabrication. The piezoelectric target scanner has been demonstrated in a raster scan pattern that should allow focused spot size measurements to begin soon after the GFI column is completed.

## 4. Design of the LMP Focusing Column

Since the LMP ion source will operate in the single accelerating lens focusing column, we will refer to this column as the LMP column.

One might expect a single lens focusing column to be simpler than a two lens column. Although it is similar in terms of parts count or alignment, the complexities related to the high voltage more than offset these. Figure II-7 is a schematic of the LMP column. The outer vacuum enclosure is basically a high voltage insulator (upper section) and a target chamber (lower section). The piezoelectric target scanner and XYZ target positioner are identical to those in the GFI column. These components will be shared by both columns for the first tests.

The target chamber and high voltage insulator are existing Hughes equipment and will be used without modification. The insulator has brazed flanges at each end and is a very rigid assembly. The lower flange, which will be operated at ground potential, supports the downstream element of the accelerating lens. The upper flange of the insulator will be operated at 60 to 100 kV. It supports a new LMP ion source assembly which protrudes deeply into the cylindrical insulator. The end cap of this assembly is the upstream element of the accelerating lens. The high voltage (100 kV) standoff requires the long mechanical paths between the two lens elements. These elements will be aligned mechanically during setup. The axis formed by their centers will then be the ion optical axis of the column. With the column in operation the LMP source will be positioned in X and Y to align with the lens axis. This provision to move the source with the high voltage on, plus several other requirements led us to abandon

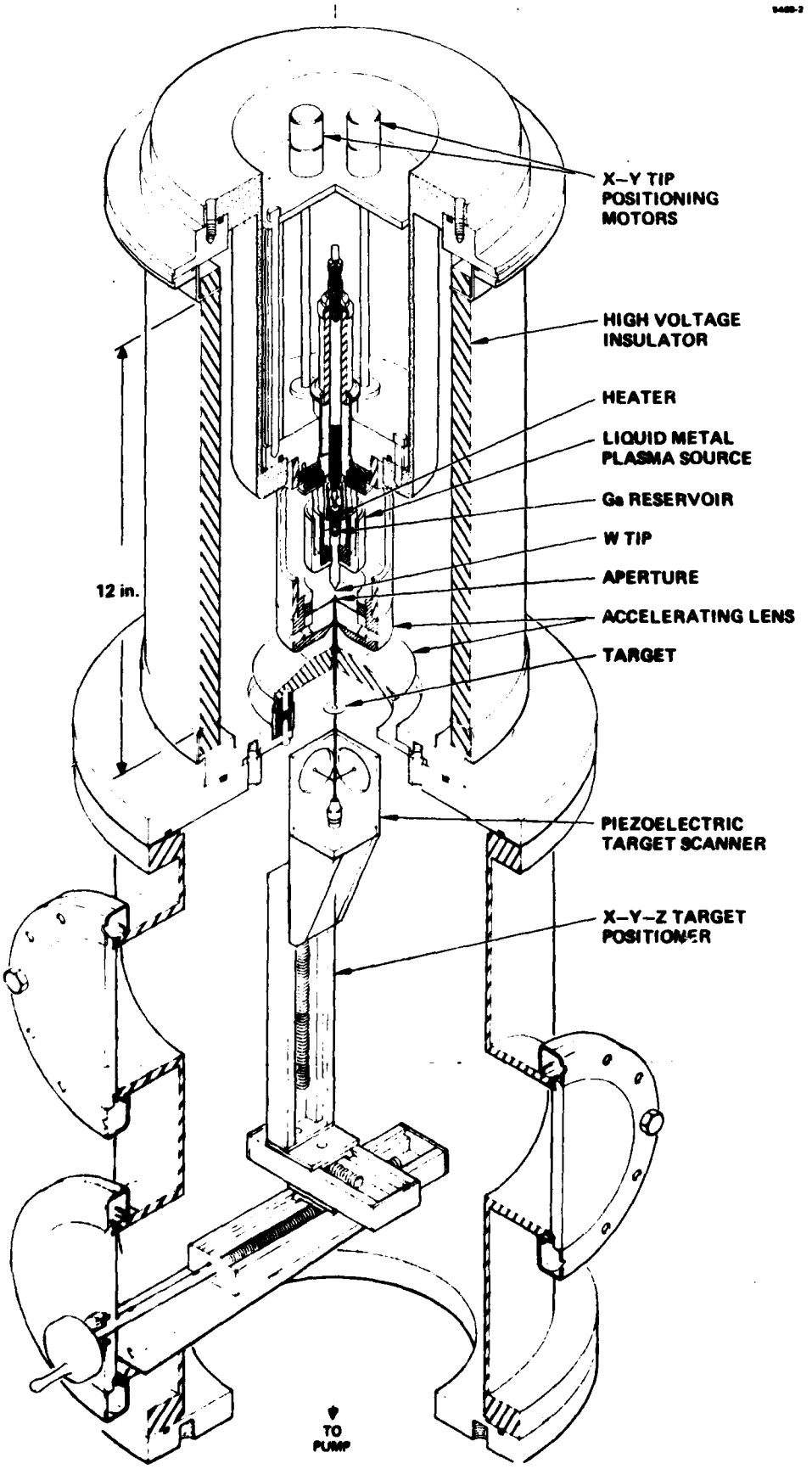


Figure II-7. LMIP focusing column.

the purchased LMP source and redesign one that would be more suitable for imaging. This redesign is part of Task E (Component Optimization) of the program. It is described in detail in the following section.

## C. Redesign of the LMP Ion Source

The LMP ion source was redesigned to:

- Support the Ga reservoir through rigid structure
- Support the tungsten needle inside the reservoir
- Relocate the reservoir heater to inside the reservoir
- Enable XY positioning of the needle (and reservoir) from outside the vacuum system with all the voltages on.

Clearly, these objectives are not intended to change source operation (e.g., the Ga feed or ionization mechanism), but rather to stabilize source location (i.e., reduce vibrational motion) and to enable accurate XY positioning.

Figure II-8 is a schematic of the redesigned LMP source assembly. This assembly is inserted into the high voltage insulator from the top (i.e., the high voltage end). The re-entrant tube that fastens to the insulator is part of the vacuum enclosure. The re-entrant tube has accurately machined reference surfaces that locate the ion source mounting flange. Thus, the ion source assembly can be removed and replaced while the alignment of the accelerating lens elements is maintained. The main mechanical support for the Ga reservoir is provided by a glass-ceramic insulator in which the reservoir tube is inserted. This insulator is supported by two moveable plates (the Y-plate and X-plate); this enables reservoir and needle to be positioned transversely. Each plate pivots on an off-axis dowel pin and is driven by an off-axis cam. The XY cam drive shafts penetrate the ion source mounting flange through O-ring seals and are coupled to stepping motors. An optical link will be used to control the stepping motors across the high voltage. In a bench test of this cam drive, positioning increments

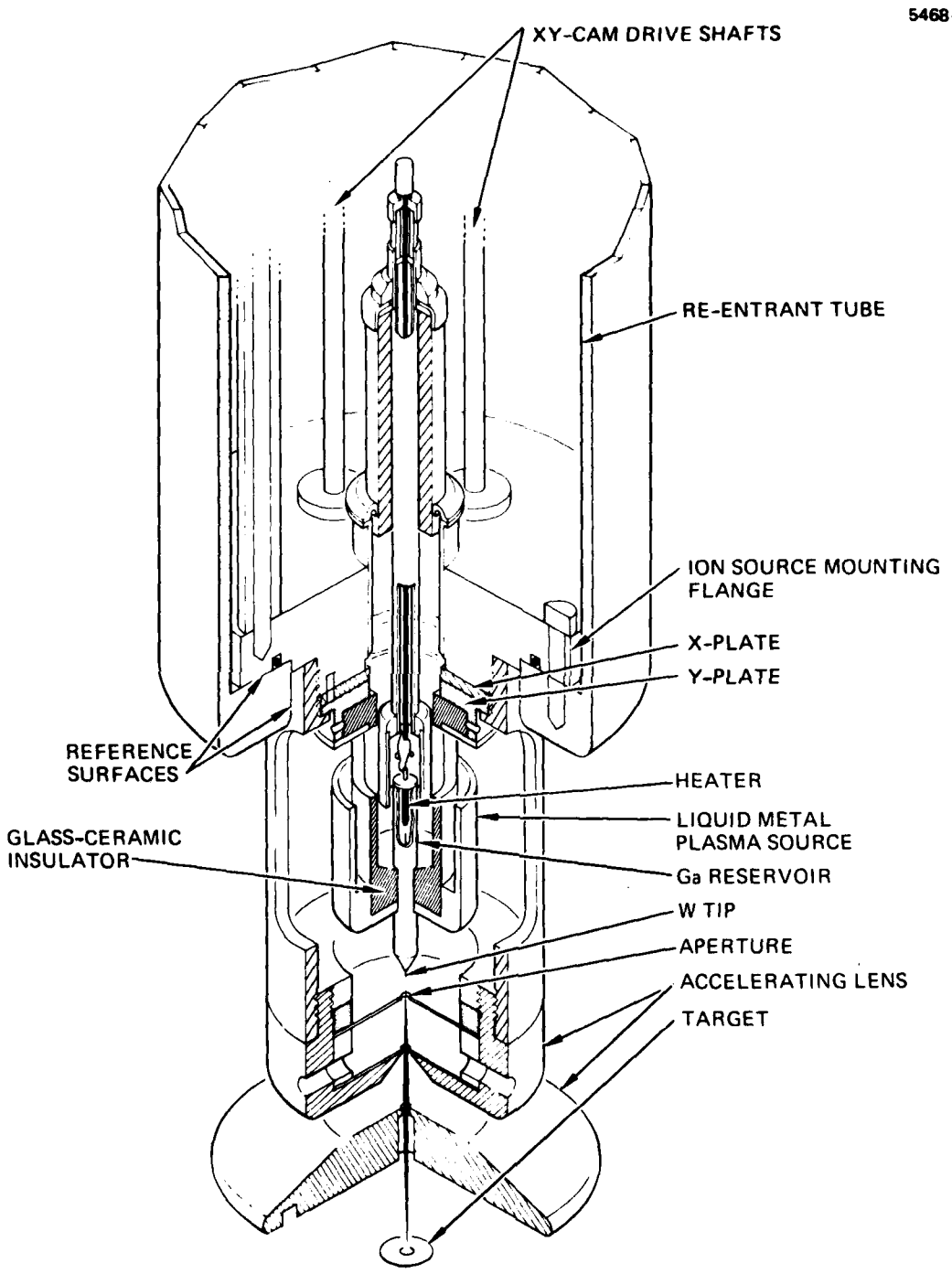


Figure II-8. Redesigned LMP ion source.

of 0.0003 in. were demonstrated. It is expected that even higher resolution positioning will be achievable.

The Ga heater to be compatible with the new design, was relocated to the inside of the reservoir tube. Here, the heater will require minimum power as compared to the old radiant heater and, therefore, thermal motion of the mechanical assembly will be minimized. The heater leads are flexible to allow XY motion; they are brought out of the vacuum through a coaxial feedthrough. The tungsten needle will be clamped inside the reservoir, but the design for doing this is not yet complete.

Upon completion, the new LMP source will first be tested in a bell jar to compare its performance with that of the purchased LMP source. After satisfactory performance is achieved, the new source will be setup in the LMP focusing column for thorough evaluation.

# III. ANALYTICAL INVESTIGATIONS

Analytical models of ion beam focusing columns will be used on this program to predict and later to optimize focusing column performance. The progress made to date in this analysis includes obtaining and running all of the necessary computer programs, and applying these programs to determine the theoretical performance of the two elementary focusing columns that are under construction. Later in the program, more complex focusing columns (e.g., those including both an accelerating lens and an einzel lens) will be analyzed in the search for an optimized ion beam focusing column for microfabrication.

## A. Lens Aberrations

The dominant lens aberrations for einzel and accelerating lenses are chromatic and spherical. This section will (1) define these aberrations, (2) describe how they can be calculated, and (3) show how final spot size and beam current are related to these aberrations and to ion source brightness.

### 1. Chromatic Aberration

The focal length of an electrostatic lens is a function of the axial velocity of the beam particles. Lower velocity particles focus in a shorter distance than higher velocity particles. This lens effect is chromatic aberration. In an attempt to focus a laminar beam of non-uniform axial velocity to a point, chromatic aberration would cause trajectories to cross and the image to be a finite size spot, as shown in Figure III-1. The axial velocity spread (energy spread) of concern here is due to random fluctuations in the emitted velocity at the source and not to time variations in the beam accelerating potential (i.e., power supply ripple). These time variations produce a time varying but uniform cross-sectional axial beam velocity. The focus would then be at a point whose location fluctuates in time.

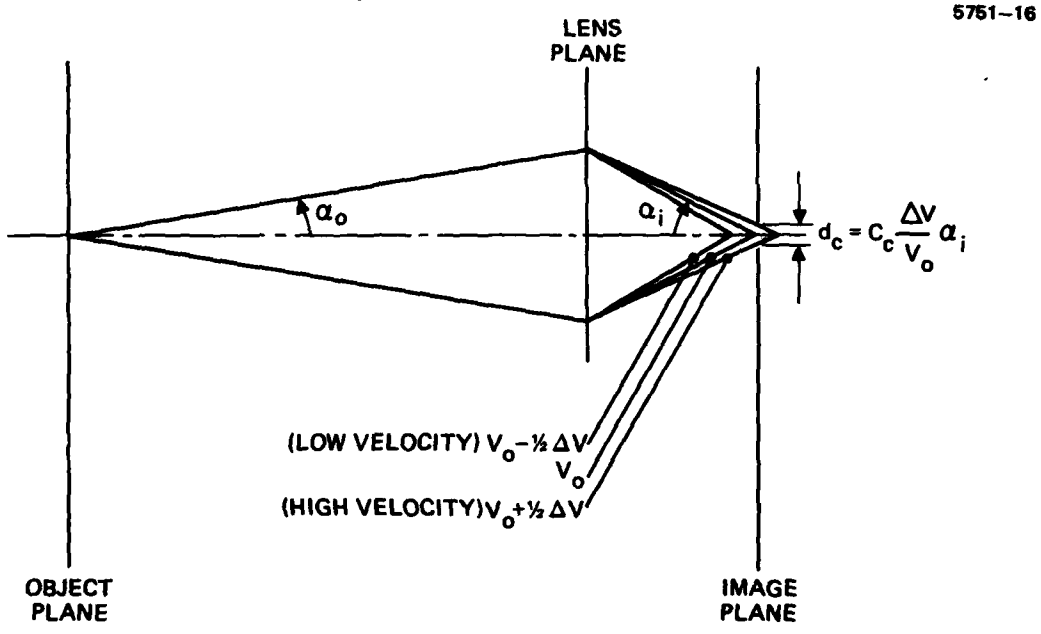


Figure III-1. Effect of chromatic aberration on beam focusing.

The spot diameter of a beam focused by a lens with a chromatic aberration coefficient $C_c$ can be referred to either the object or image plane. For the latter case, the spot diameter is given by

$$d_i = C_{c_i}\left(\frac{\Delta V}{V_o}\right)\alpha_i \quad , \tag{III-1}$$

where $\Delta V$ is the magnitude of the total axial energy spread, $eV_o$ is the nominal axial energy, and $\alpha_i$ is the convergence half-angle of the beam at the image.*

Similarly, using the same notation as above, the diameter $d_o$ of the disc of least confusion referred to the object plane is given by

$$d_o = C_{c_o}\frac{\Delta V}{V_o}\alpha_o \quad , \tag{III-2}$$

when $\alpha_o$ is the semi-angle of divergence at the object position. For the zero ($\alpha_o = 0$) magnification case, $Cc_i$ must be used; for the infinite ($\alpha_i = 0$) magnification case, $Cc_o$ must be used. For finite magnification, either formula can be used since $Cc_i = M^2 Cc_o$; however, it is preferable to use $Cc_i$ for a de-magnifying lens and $Cc_o$ for a magnifying lens.

### 2. Spherical Aberration

Spherical aberration, although not as important as chromatic aberration, does contribute significantly (at higher beam angles) to the spot size for both lens columns. The effect of spherical aberration is illustrated in Figure III-2. Rays entering the lens are focused at a distance which decreases with the radial distance at which they pass through the lens. This aberration causes trajectories to

*Some workers use $2\Delta V/V_o$ where $\Delta V$ refers to half the total energy spread.

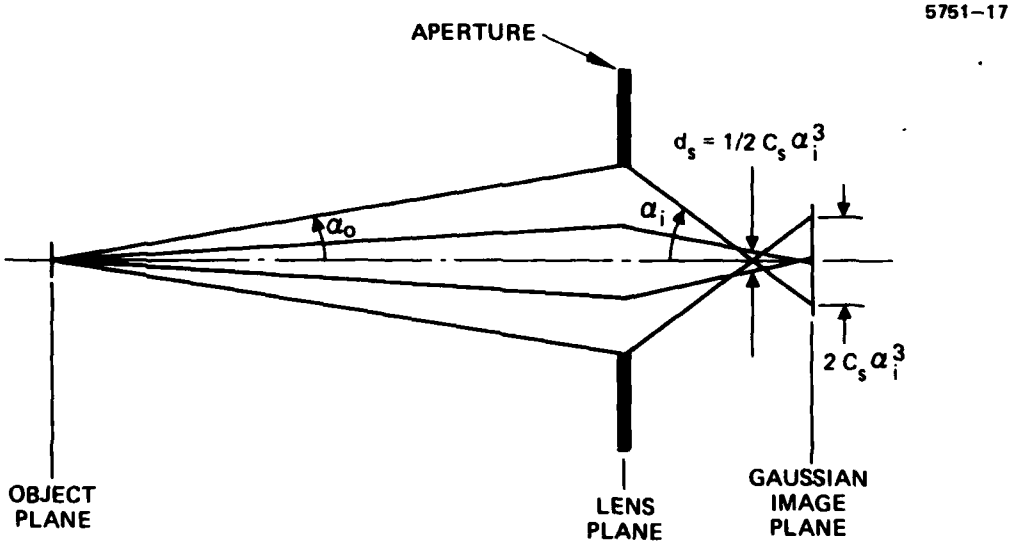


Figure III-2. Effect of spherical aberration on beam focusing.

cross and produces a disc instead of a point focus. The minimum beam diameter (disk of least confusion) occurs in front of the Gaussian image plane and can be referred to either the object or the image plane. For the latter case,

$$d_i = \frac{1}{2} C_{s_i} \alpha_i^3 \quad , \qquad \text{(III-3)}$$

where $\alpha_i$ is the image convergence half-angle and $C_s$ is the spherical aberration coefficient of the lens. When the disc of confusion is referred to the object plane, the analogous formula becomes

$$d_o = \frac{1}{2} C_{s_o} \alpha_o^3 \quad , \qquad \text{(III-4)}$$

where $\alpha_o$ is the semi-angle of divergence at the object position. As with the chromatic aberration, $Cs_i$ must be used for zero magnification and $Cs_o$ must be used for infinite magnification. For finite magnification, since $M = \alpha_o/\alpha_i$ and $d_o = Md_i$, the two coefficients are related by

$$Cs_o M^4 = Cs_i \quad . \qquad \text{(III-5)}$$

B. Calculation of Aberration Coefficients

A three part computer program developed by Munro[5,6] was obtained for calculating the aberration coefficients $C_c$ and $C_s$. The program (1) calculates the axial potential V(z) through the lens for a given lens configuration (e.g., electrode shapes and spacings); (2) uses V(z) to calculate characteristic trajectories $r_o(z)$ and $R_o'(z)$ through the lens; and (3) uses V(z), $r_o(z)$, $r_o'(z)$, and an object position $z_o$ to calculate the spherical and chromatic aberration coefficients Cs and Cc, the focal length f, and the image position $z_i$.

After the axial potential V(z) is calculated, paraxial electron trajectories r(z) are then computed numerically, using a fourth-order Runge-Kutta formula to solve the paraxial ray equation

$$r'' + \frac{V'}{2V} r' + \frac{V''}{4V} r = 0 \quad , \tag{III-6}$$

where V(z) is the axial potential distribution and primes denote differentiation with respect to z. The spherical and chromatic aberration coefficients, referred to the object plane $z_o$ or the image plane $z_i$, are then computed numerically by using Simpson's rule to evaluate the aberration integrals

$$C_s = \frac{1}{16\sqrt{V_\alpha}} \int_{z_o}^{z_i} \left\{ \left[ \frac{5}{4}\left(\frac{V''}{V}\right)^2 + \frac{5}{24}\left(\frac{V'}{V}\right)^4 \right] r_\alpha^4 \right. \tag{III-7}$$

$$\left. + \frac{14}{3}\left(\frac{V'}{V}\right)^3 r_\alpha' r_\alpha^3 - \frac{3}{2}\left(\frac{V'}{V}\right)^2 r_\alpha'^2 r_\alpha^2 \right\} \sqrt{V}\, dz \text{ and}$$

$$C_c = \sqrt{V_\alpha} \int_{z_o}^{z_i} \left( \frac{1}{2}\frac{V'}{V} r_\alpha' + \frac{1}{4}\frac{V''}{V} r_\alpha \right) \frac{r_\alpha}{\sqrt{V}}\, dz \quad , \tag{III-8}$$

where $V_\alpha = V(z_o)$, $r_\alpha(z_o) = 0$, and $r_\alpha'(z_o) = 1$ if the aberration coefficients are referred to $z_o$ or $V_\alpha = V(z_i)$, $r_\alpha(z_i) = 0$, and $r_\alpha'(z_i) = -1$ if the aberration coefficients are referred to $z_i$. Magnification, whether low or high, is calculated from the formula

$$M = \frac{\alpha_o}{\alpha_i}\sqrt{\frac{V_o}{V_i}} \quad , \tag{III-9}$$

where $\alpha_o$ and $\alpha_i$ are the convergence angles of the trajectory and $V_o$ and $V_i$ are the corresponding voltages at $z_o$ and $z_i$, respectively.

This lens analysis was implemented on our computer. To check the programs, Munro's test cases were run; they gave identical results. In addition, the bell-shaped potential distribution for Glasser's[7] lens was input to the computer program and the computed results were compared with their closed form values as obtained by Kanaya.[8] For this test case, the axial potential

$$V(z)/V_o = 1 - \frac{k^2}{1 + \left(\frac{z}{d}\right)^2} \qquad \text{(III-10)}$$

was used with $k^2 = 0.8$. This potential is symmetric about $z = 0$ and is initially decelerating. The parameter d is the half-width of the bell-shaped distribution; the parameter $k^2$ fixes the lens strength. Figure III-3 shows the excellent agreement between the calculated results and the closed-form solutions. Lens parameters $C_s$, $C_c$, and f were also computed for the Electros einzel lens that we purchased. Figure III-4 compares the computed parameters with the experimentally measured values. The computed and experimental values of $C_s$ and f agree quite well (within an average of ~10%). However, the computed values of $C_c$ differ by up to ~40% from the measured value. The latter difference can probably be accounted for by the experimental difficulties involved in measuring the energy spread of an operating source. (The experimental results presented in quarterly report No. 1 for this lens were inadvertently plotted for the wrong lens.)

## C. Beam Column Analysis

### 1. Calculation of Spot Size

The spot diameters for both the double einzel and single lens accelerating column were calculated by adding in quadrature the chromatic and spherical aberration terms to the effective source size. The justification for this procedure is shown in Ref. 10, where it is proven that all uncorrelated circularly symmetric aberrations add

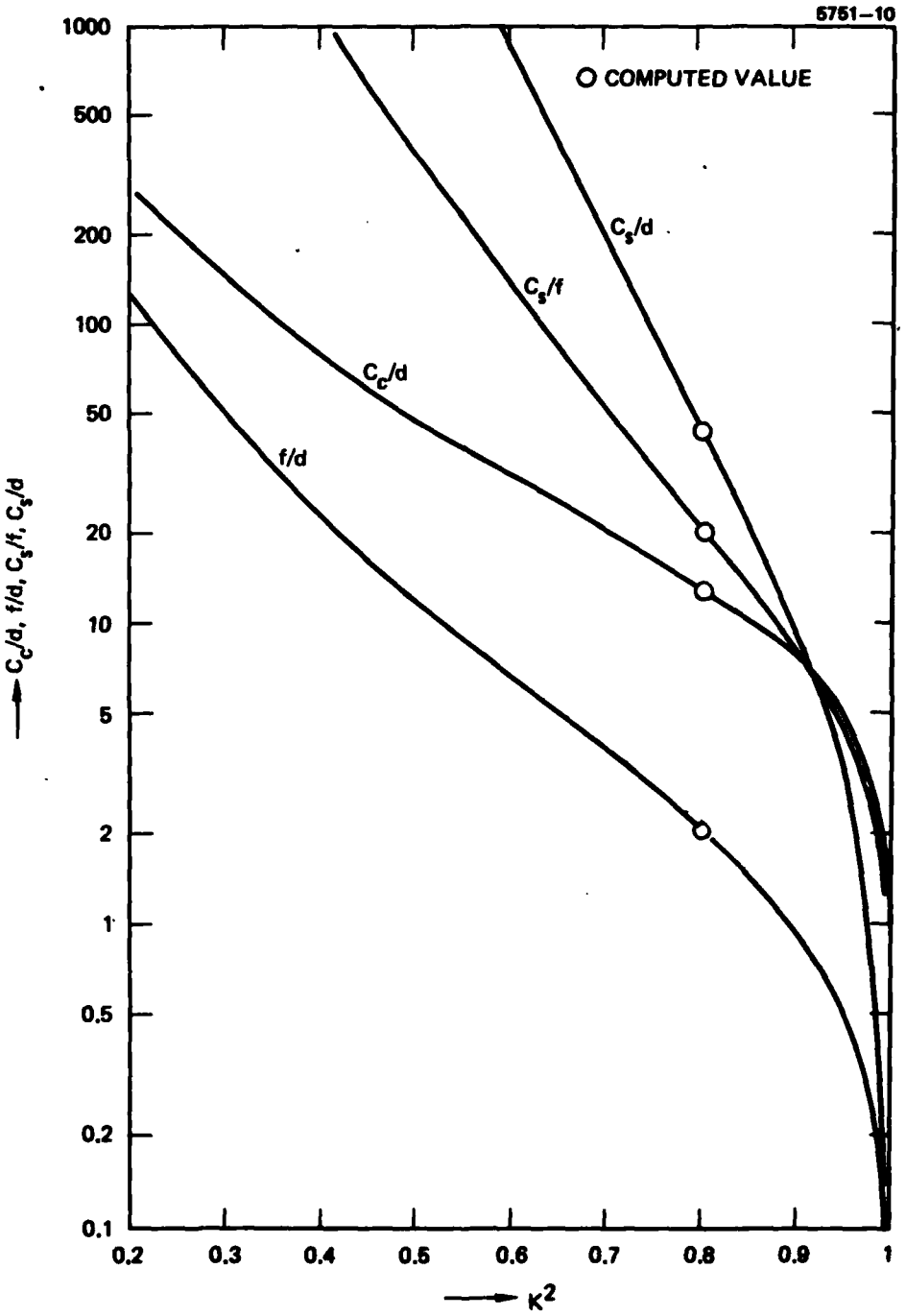


Figure III-3. Theoretical focal length and chromatic and spherical aberration constants for Glasser einzel lens along with computed values using Munros computer program.

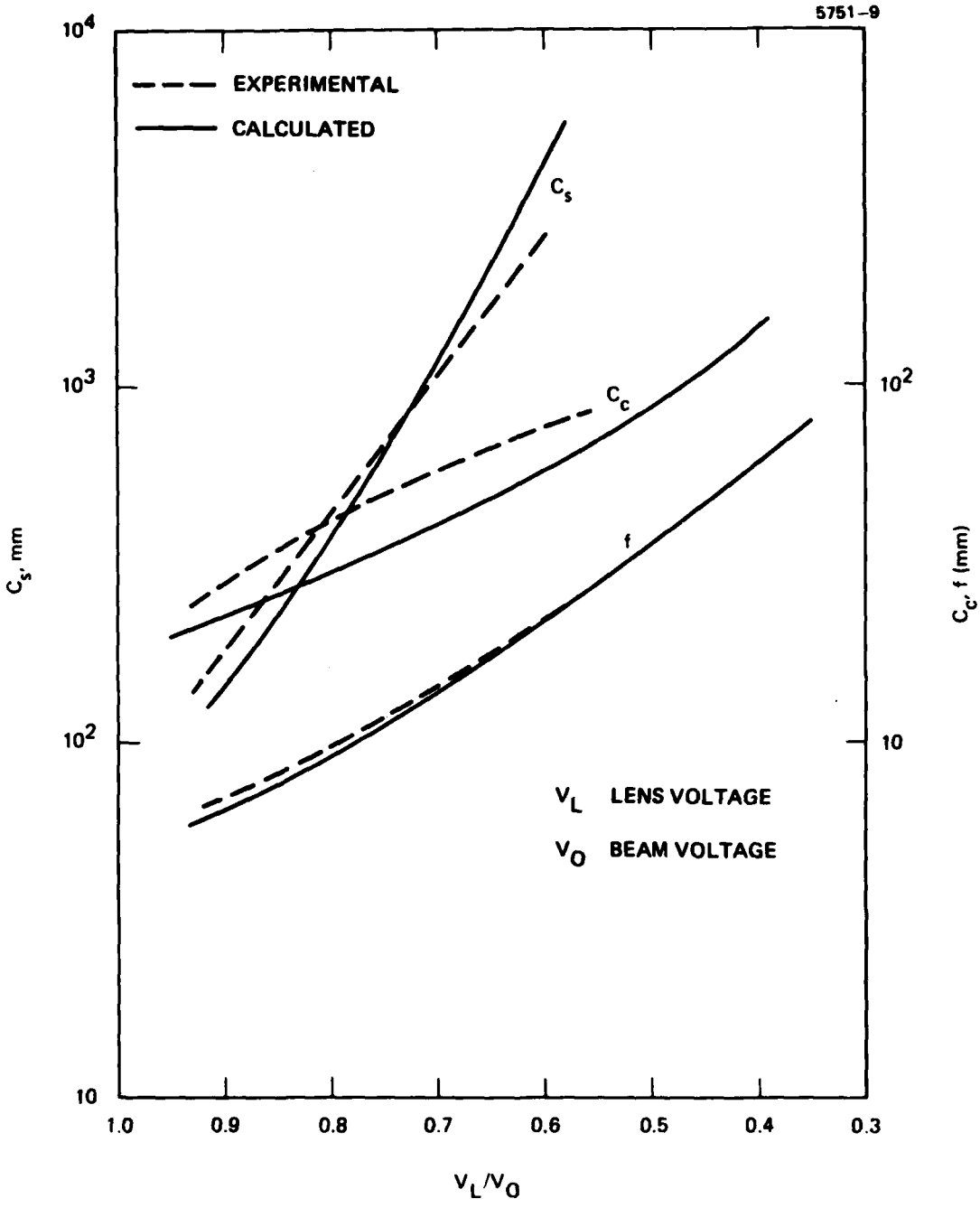


Figure III-4. Comparison of experimental and calculated parameters for GFI focusing column einzel lens.

quadratically provided the radius of the aberration disk is defined as the square root of the normalized second moment of the current density distribution. Thus, for the single lens accelerating column, the spot diameter $d_s$ was calculated as

$$d_s^2 = \left\{ d_o^2 + \left[ \frac{1}{2} Cs_o \alpha_o^3 \right]^2 + \left[ Cc_o \frac{\Delta V}{V} \alpha_o \right]^2 \right\} M_1^2 \quad , \qquad \text{(III-11)}$$

where $d_o$ is the effective source size and the aberration terms referred to the object plane are as previously defined. For the double einzel lens column, the first lens contributes the spot size given by Eq. III-11 which is then demagnified by the second lens an amount $M_2$. The aberration contributions for the second lens referred to the image plane must also be added so that

$$d_s^2 = \left[ d_o^2 + \left( \frac{1}{2} Cs_o \alpha_o^3 \right)^3 + \left( Cc_o \frac{\Delta V}{V} \alpha_o \right)^2 \right] (M_1 M_2)^2$$

$$+ \left( \frac{1}{2} Cs_i \alpha_i^3 \right)^2 + \left( Cc_i \frac{\Delta V}{V} \alpha_i \right)^2 \quad , \qquad \text{(III-12)}$$

where $M_1 M_2$ is the total magnification and $\alpha_i = \alpha_o/(M_1 M_2)$.

Since spot size is a function of angular aperture $\alpha_o$, it is convenient to plot spot size as a function of this parameter. To do this it is necessary to pick a lens strength and object position, since the aberration coefficients are functions of these parameters.

## 2. Spot Current Calculation

It is customary[11] to assume for field emitters, that the source emits uniformly into one steradian so that the probe current $I_p$ is given in terms of the tip current $I_{tip}$ and semi-angle $\alpha_o$ at the emitter:

$$I_p = I_{tip} \pi \alpha_o^2 \quad . \qquad \text{(III-13)}$$

In terms of the source brightness $B_s$ and effective source radius $r_1$,

$$I_{tip} = B_s \pi r_1^2 \quad . \tag{III-14}$$

For the GFI source and using B = $10^8$ A/cm$^2$ - sr, $2r_1$ = 10 Å ($10^{-7}$ cm), and Eq. III-14 we have

$$I_{tip} = 10^8 \frac{\pi}{4} (10^{-7})^2 \times 10^6 \frac{\mu A}{A} = 0.785 \ \mu A/sr \quad .$$

Similarly for the LMP source using B = 1.4 x $10^6$ and $2r_1$ = 500 Å ($5 \times 10^{-6}$ cm) we have

$$I_{tip} = 1.4 \times 10^6 \frac{\pi}{4} (5 \times 10^{-6})^2 \times 10^6 = 27.5 \ \mu A/sr \quad .$$

For a 10 mrad beam half-angle, the corresponding probe currents using Eq. III-13 are 0.25 nA for the GFI source and 8.6 nA for the LMP source.

## D. Theoretical Column Performance

After analyzing several lenses, the analytical investigation was directed toward evaluating the simple focusing columns for the GFI and LMP ion source testing. Three columns were considered: single and double einzel lens columns and a single accelerating lens column. A computer program was written to plot focused spot diameter versus beam half-angle at the object $\alpha_o$ using Eq's. III-11 or III-12. Figure III-5 shows the results if the source is imaged by one of the einzel lenses. At $\alpha_o$ = 10 mrad, the spot size exceeds 1 μm and is unacceptable. Although this single-einzel lens column was rejected although it would be relatively simple to construct. The next column considered was a twin einzel lens configuration. The first lens collimates the beam, and the second lens then demagnifies it to a small spot. In this mode, both lenses can operate near full strength (e.g., $V_L/V_c \sim 1$) where the aberration coefficients are minimum. Figure III-6 shows the computed

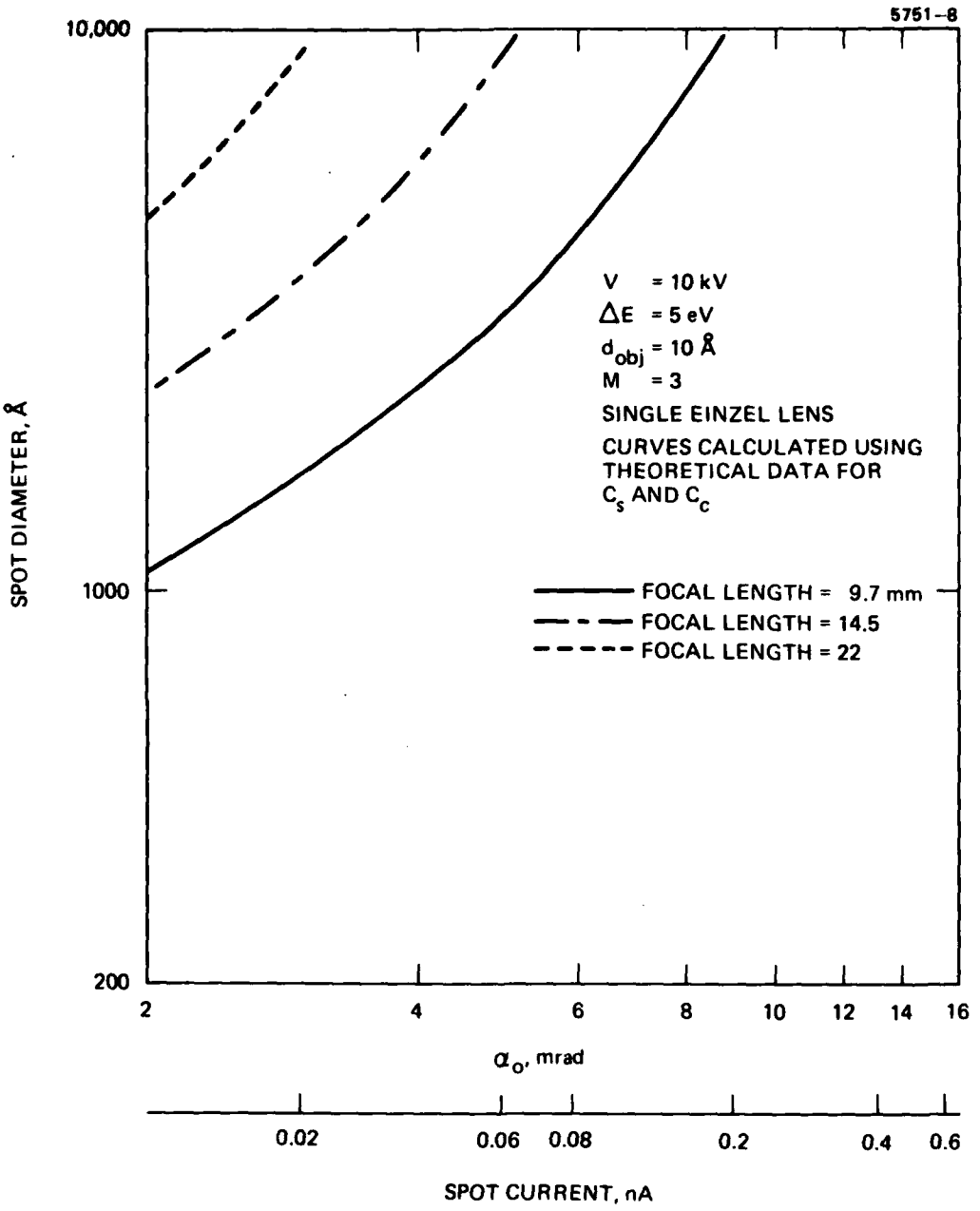


Figure III-5. Performance of a single-einzel lens column.

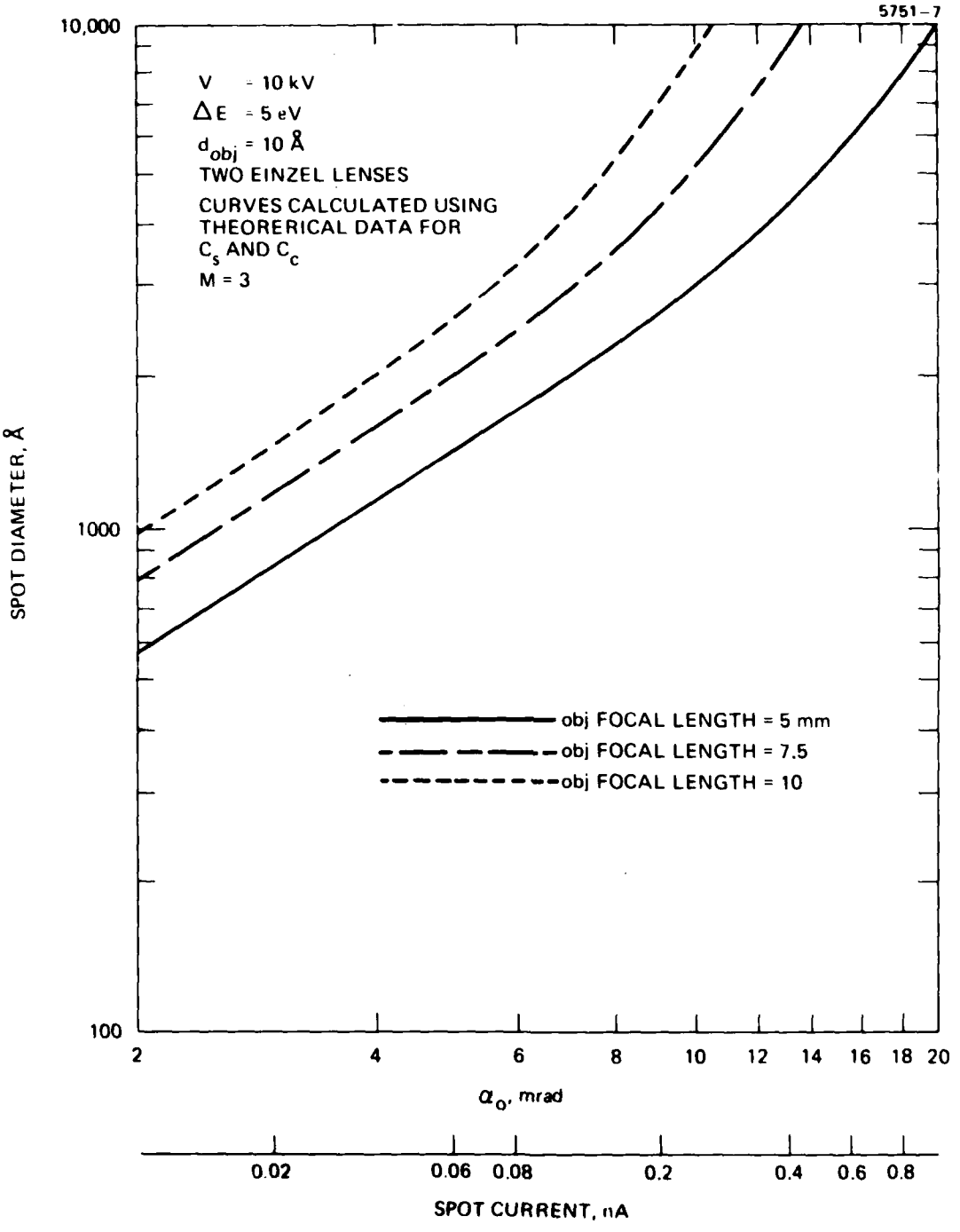


Figure III-6. Performance of a double-einzel lens column.

performance of the two einzel lens column, assuming Electro's einzel lens and the GFI source parameters ($B = 10^8$ A/cm$^2$ sr, $\Delta V$ = 5 eV, $d_{obj}$ = 10 Å). At $\alpha_o$ = 10 mrad and M = 3, the predicted spot current is 0.25 nA. Here, the smallest objective focal length 5 mm is chosen for minimum aberrations and M = 3 is chosen for a reasonable working distance (~10 mm). Based on the predicted 2800 Å spot, the two-einzel lens column is suitable for experimental evaluation. The third column considered employs an accelerating lens to focus the beam. The actual lens configuration chosen was designed by Munro and shown to have lower aberration coefficients than the Crewe lens. Figure III-7 shows the performance of the Munro lens (hybrid lens No. 1) assuming the LMP source parameters given by Krohn ($\Delta E$ = 12 eV, $d_{obj}$ = 500 Å and $B = 1.4 \times 10^6$ A/cm$^2$ sr). A voltage ratio of 10:1 is also assumed, which means that the final beam voltage will range between 60 and 80 kV for the typical extraction voltages of 6 to 8 kV. The aberrations of this accelerating lens are lower than those of einzel lenses and do not become important until $\alpha_o$ approaches 10 mrad. For smaller $\alpha_o$, spot size is basically determined by the product of the magnification M and the source size $d_{obj}$. The predicted spot size and current at $\alpha_o$ = 10 mrad and M = 1 are about 2000 Å diameter and 8.6 nA, respectively. The higher current in comparison to the GFI source (~0.25 nA) is due to the larger active source area, about 500 Å diameter, for the LMP source is compared to the very small 10 Å diameter for the GFI source. If the assumed LMP source parameters and lens performance are experimentally correct, it should be possible to focus 1 nA of current into a 500 Å diameter spot. The current density in the spot would be ~51 A/cm$^2$, which corresponds to a very practical spot implantation rate of $3.2 \times 10^{14}$ ions/cm$^2$ per microsecond. These predictions are very encouraging.

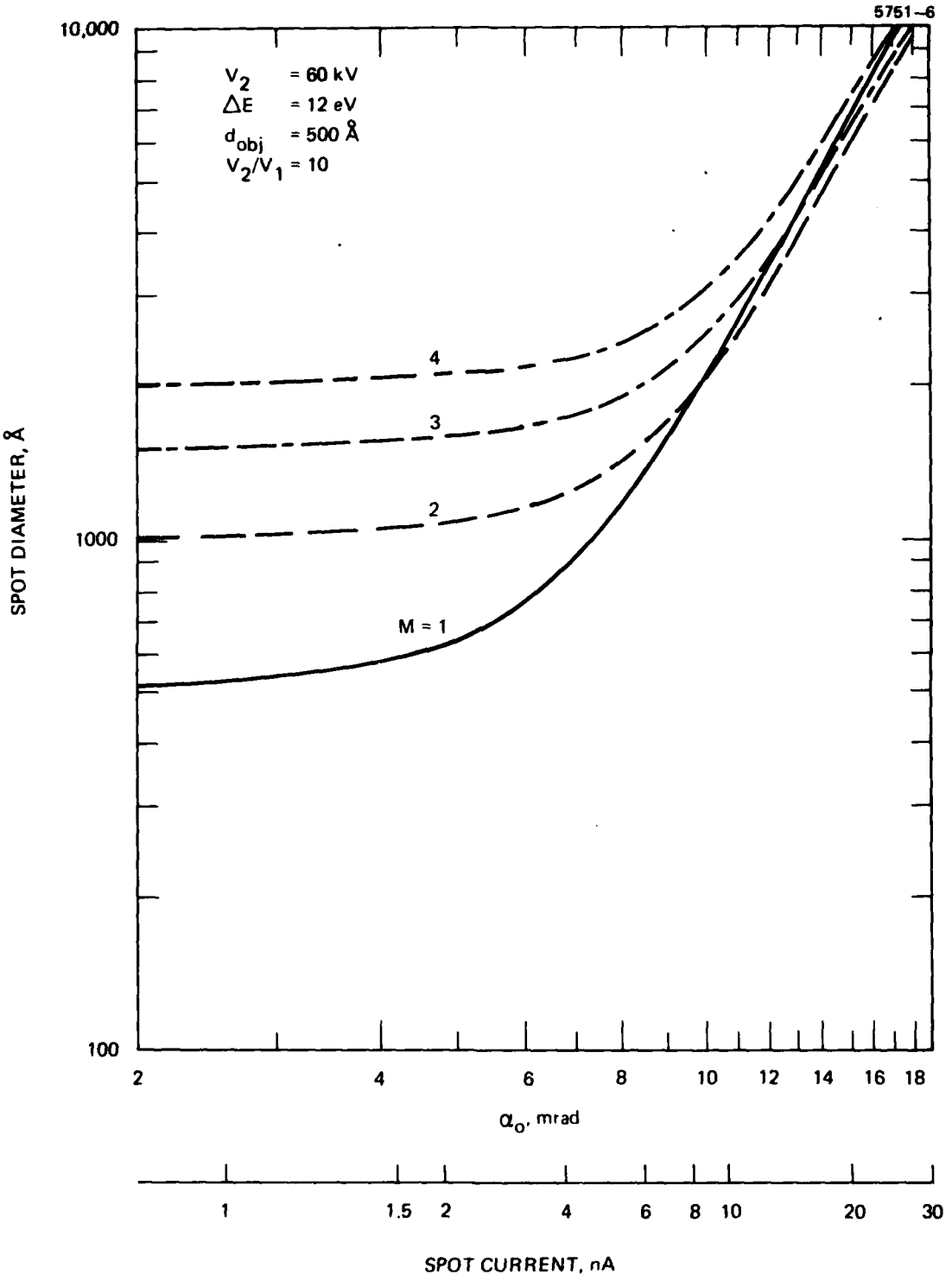


Figure III-7. Performance of an accelerating lens column.

## E. Literature Survey

A part of the analytical investigation, a literature survey is being made to uncover the best candidate column components from which an optimized column can be designed. Survey results thus far include many references related to sources, lenses, and focusing columns. The list of references is presented in Appendix B. It has already been very useful in the decision on which experimental focusing columns should be built. The literature will be continued throughout the program.

## SECTION IV

## CONCLUSIONS AND PLANS FOR NEXT QUARTER

The program activities during the first six months are in good general agreement with the proposed phasing schedule. The consideration of electrostatic beam deflection has been postponed temporarily (in the literature search and in the experimental focusing columns) to allow concentrating on focusing the beam to a small spot. On the other hand, the component optimization task was begun early because it was necessary to redesign the LMP source for our focusing application.

During the next quarter, the remaining components of the focusing columns will be designed and fabricated. These include the XYZ stage, piezoelectric scanner, beam defining apertures for the lenses, secondary electron detector, gallium reservoir, and cam drive mechanism. It is anticipated that the GFI column will be completed first and its initial turnon will occur during the next quarter. The literature survey and performance analysis will continue, and the beam column design optimization task will begin.

## V. FINANCIAL STATUS

Manhours expended in the second quarter: 1,818.5 hours
Total second quarter costs: Mfg. Cost 54.2 K

Total manhours expended to date: 11/26/76 2857.5 hours
Total costs to date: Mfg. Cost 89.2 K

Estimated period covered by allocated funds: to 9-1-77

## REFERENCES


1. E.W. Muller and T.T. Tsong, Field Ion Microscopy, Principles and Applications, Elrewer Publishing Co., New York (1969).

2. A.V. Crewe, J. Wall, and C.M. Welter, "Electron Gun Using a Field Emission Source," Rev. Sci. Instrum. 39, No. 4, 576 (1968).

3. Coats and Welter, Electron Microscope (Commercial Brochure).

4. J.E. Wolfe, "An Electron Gun for Data Storage Micromachining," unpublished.

5. E. Munro, "Computer-Aided Design of Electron Lens by the Finite Element Method," (in Image Processing and Computer — aided design in Electron Optics, Academic Press, 1973, p. 284, edited by P. Hawkes).

6. E. Munro, "A Set of Computer Programs for Calculating the Properties of Electron Lenses," Cambridge University Engineering Department Report, January 1975.

7. W. Glasser and P. Schiske, Optik 11, 422-467 (1954).

8. K. Kanaya, et al., J. Sci. Inst. 3, 416 (1966).

9. A. Crewe, et al., "A Simple Scanning Electron Microscope," Rev. Sci. Instrum. 40, 241 (1969).

10. K. Harte, "Theory of Aberration Mixing in Electron-Optical Systems," J. Vac. Sci., Tech. 10, 1098 (1973).

# APPENDIX A

## TUNGSTEN NEEDLE FABRICATION

Tungsten needles for the LMP source are formed by electro-chemically etching points on 0.254 mm diameter tungsten wire. The wire should be inspected for longitudinal cracks and striations on the surface. The wire is straightened by putting tension on the wire and applying voltage from a variac to opposite ends until the wire glows red. The voltage is then decreased while tension is maintained. The wire is then cut to lengths of 45 to 50 mm using an abrasive-type cut-off wheel to avoid splitting the ends. Surface striations and roughness should be removed by electro-polishing. Figure A-1 is a schematic of the needle-forming apparatus.

The wire is mounted vertically above the electrolyte with the end immersed 2 to 3 mm in the solution. Four volts ac is applied between the tungsten wire and the anode until the electrolyte around the wire stops bubbling. This step forms a submicrometer radius point such as is shown in Figure A-2.

The needle is again immersed in electrolyte to two-thirds its length and 4 V ac is applied for 10 sec. This "blunts" the submicrometer point, forming a finished 5 μm radius point as shown in Figure A-3.

Immediately before the needle is installed in the source it is clean fired in a wet hydrogen furnace at 1000°C for 15 min. After cooling, it is placed in clean liquid gallium until the surface of the needle, and particularly the point, is thoroughly wetted with an even layer of gallium. At that point the needle is ready to be installed in the reservoir of the LMP source.

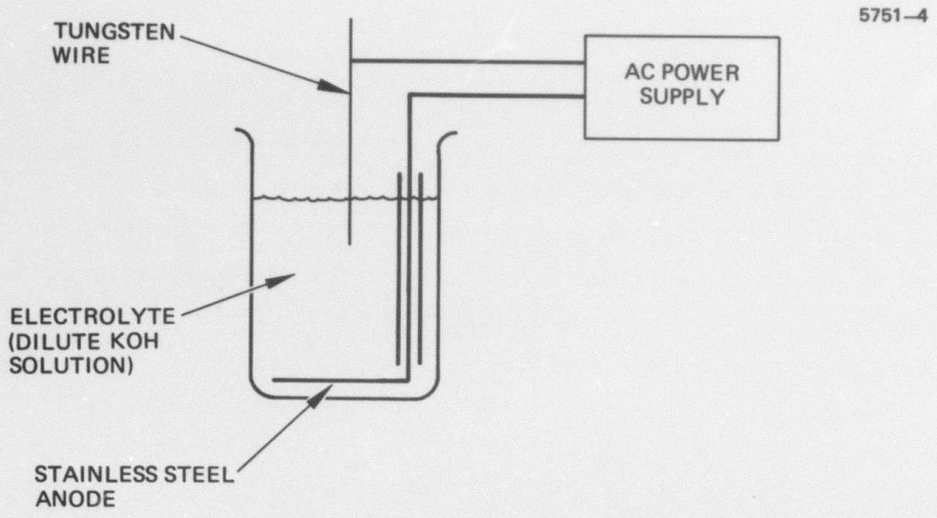


Figure A-1. Needle forming apparatus – schematic diagram.

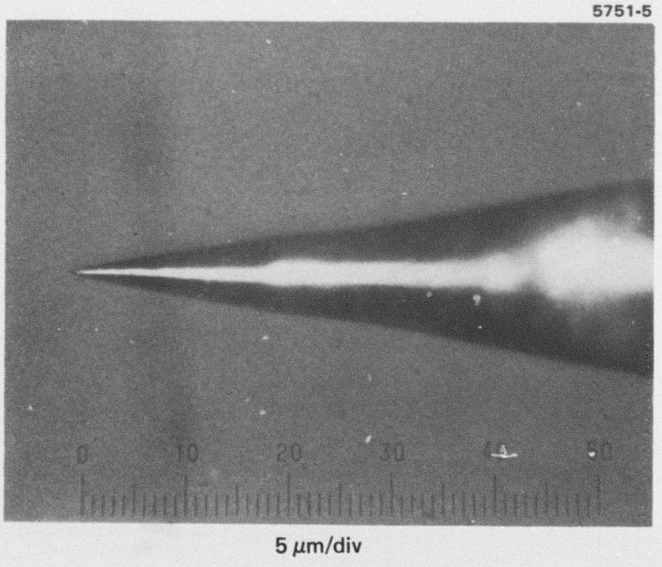


Figure A-2. Tungsten needle with a submicrometer radius tip.

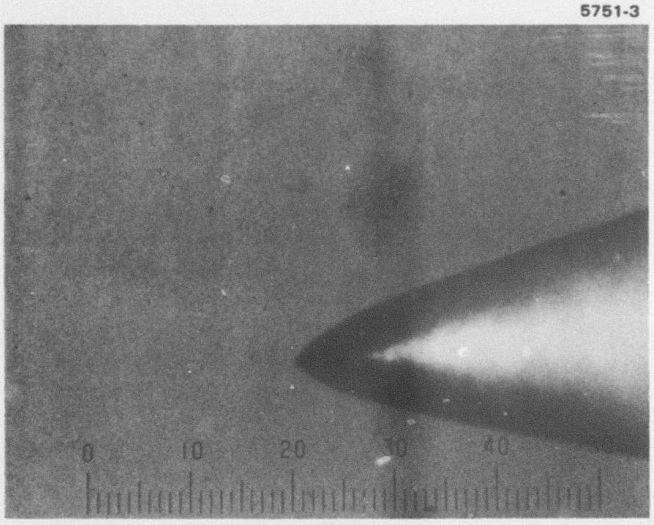


Figure A-3. Tungsten needle with a 5 μm radius tip.

# APPENDIX B

## LITERATURE SURVEY

This appendix lists the references that have been identified and examined to this point in the literature survey. At the end of the program, copies of the papers will be delivered.

### Lenses

#### Einzel


G. V. Der-Shvarts and I. S. Makarova, "Study of Spherical Aberrations of Axisymmetric Einzel-Lenses," Radio Engr. and Electron. Phys. 11, No. 10, 1581 (1966).

G. V. Der-Shvarts and I. S. Makarova, "Axially-Symmetric Single Lenses with Small Third Order Spherical Aberration," Radio Engr. and Electron. Phys. 14, No. 2 (1969).

Von W. Glaser and P. Schiske, Wien, "Strenge Durchrechnung einer typischen electrostatischen Einzellinse," Optik 11, 422 (1954).

Von F. Heise, "Bestimmung von Verzeichnung und Öffnungsfehler electrostatischer Linsen aus Hauptflächen und Brennpunkt-Hilfsflächen," Optik 5, 479 (1949).

K. Kanaya, H. Kawakatsu, H. Yamazaki, and S. Sibata, "Electron Optical Properties of Three-Electrode Electron Lenses," J. Sci. Instrum. 43, 416 (1966).

P. Kostka, "The Calculated Properties of a Three-Electrode 'Single' Lens," Nucl. Instrum. Methods 91, 413-415, North-Holland Publishing Co. (1971).

Von R. Seeliger, "Ein Neues Verfahren zur Bestimmung des Öffnungsfehlers von Electronenlinsen," Optik 4, 258 (1948).


#### Accelerating


K. Kuroda, H. Ebisui, and T. Suzuki, "Three-Anode Accelerating Lens System for the Field Emission Scanning Electron Microscope," J. Appl. Phys. 45, 2236 (1974).

K. Kuroda and T. Suzuki, "Three-Anode Accelerating Lens System for Field Emission Scanning Electron Microscopy (II)," Appl. Phys. Lett. 25, No. 1, 23 (July 1974).

K. Kuroda and T. Suzuki, "Analysis of Accelerating Lens System in Field-Emission Scanning Electron Microscope," J. Appl. Phys. 45, 1436 (1974).

## Aberration Theory

G. D. Archard, "On the Spherical Aberration Constant," Rev. Sci. Instrum. 27, 1049 (1958).

A. B. El-Kareh, "Design and Analysis of Symmetrical and Asymmetrical Electrostatic Immersion Lenses Using a Digital Computer," Record of 10th Symposium on Electron, Ion, and Laser Beam Technology, (R.M. Thornley, ed.) San Francisco Press, p. 353.

D. L. Fraser, Jr., W. J. Meyers, and T. G. Elser, "A Computer Analysis of the Spherical Aberration of Three Electrostatic Immersion Lenses," Record of 11th Symposium on Electron, Ion, and Laser Beam Technology (R. M. Thornley, ed); San Francisco Press, Inc. p 209.

Von R. Seeliger, "Über die Justierung sphärisch korrigierter electronenoptischer Systeme," Optik 10, 29 (1953).

## Sources

K. T. Considine and M. M. Balsiger, "High Brightness, Long Life from New T-F Emitter," Research/Development (April 1976).

V. E. Krohn and G. R. Ringo, "Ion Source of High Brightness Using Liquid Metal," Appl. Phys. Lett. 27, No. 9 479 (Nov. 1975).

V. E. Krohn and G. R. Ringo, "Microprobe Design Using a Liquid Gallium Ion Source," Int. J. Mass Spectry. Ion Phys. (In press)

J. H. Orloff and L. W. Swanson, "Study of a Field-Ionization Source for Microprobe Applications," J. Vac. Sci. Technol. 12, No. 6, Nov./Dec. 1975.

## Columns

A. V. Crewe, M. Isaacson, and D. Johnson, "A Simple Scanning Electron Microscope," Rev. Sci. Instrum. 40, No. 2, 241, (1969).

G. V. Der-Shvarts and I. S. Gaydukova, "On the Principles of Dynamical Focusing of Microprobing Systems," Radio Engineering And Electronic Physics 13, No. 2 (1968).

L.A. Fontijn, "Some Design Aspects of an Electron Beam Micro Recording System," (Private conversation)

H. Heil, "The Very Bright Field Ionization and Field Evaporation Ion Sources. Some Uses. A Beam Formation and Scanning System," Proc. of the Symposium on Ion Sources and Formation of Ion Beams, Brookhaven Nat. Lab., October 1971.

M. Singh, J. Melvin, and Z.H. Cho, "Design Study of a 200 keV Scanning Proton Microprobe Using a Field Ionization Source," IEEE Trans. on Nuclear Science NS-23, No. 1, 657, February, 1976.

L.H. Veneklasen, "Some General Considerations Concerning the Optics of the Field Emission Illumination System," Optik 36, 410 (1972).

L.H. Veneklasen and B.M. Siegel, "Field-Emission Illumination System Using a New Optical Configuration," J. Appl. Phys. 43, 4989 (1972).